

An enriched multiscale mortar space for high contrast flow problems

Eric T. Chung*

Shubin Fu[†]Yanfang Yang[‡]

November 19, 2018

Abstract

Mortar methods are widely used techniques for discretizations of partial differential equations and preconditioners for the algebraic systems resulting from the discretizations. For problems with high contrast and multiple scales, the standard mortar spaces are not robust, and some enrichments are necessary in order to obtain an efficient and robust mortar space. In this paper, we consider a class of flow problems in high contrast heterogeneous media, and develop a systematic approach to obtain an enriched multiscale mortar space. Our approach is based on the constructions of local multiscale basis functions. The multiscale basis functions are constructed from local problems by following the framework of the Generalized Multiscale Finite Element Method (GMsFEM). In particular, we first create a local snapshot space. Then we select the dominated modes within the snapshot space using an appropriate Proper Orthogonal Decomposition (POD) technique. These multiscale basis functions show better accuracy than polynomial basis for multiscale problems. Using the proposed multiscale mortar space, we will construct a multiscale finite element method to solve the flow problem on a coarse grid and a preconditioning technique for the fine scale discretization of the flow problem. In particular, we develop a multiscale mortar mixed finite element method using the mortar space. In addition, we will design a two-level *additive* preconditioner and a two-level *hybrid* preconditioner based on the proposed mortar space for the iterative method applied to the fine scale discretization of the flow problem. We present several numerical examples to demonstrate the efficiency and robustness of our proposed mortar space with respect to both the coarse multiscale solver and the preconditioners.

1 Introduction

In this paper, we consider the following second order elliptic differential equation in mixed form:

$$\mathbf{q} + \kappa \nabla u = 0 \quad \text{in } \Omega, \quad (1a)$$

$$\nabla \cdot \mathbf{q} = f \quad \text{in } \Omega, \quad (1b)$$

$$u = 0 \quad \text{on } \partial\Omega. \quad (1c)$$

where $\Omega \subset \mathbb{R}^d$ ($d = 2, 3$) is a bounded polyhedral domain with outward unit normal vector \mathbf{n} on the boundary, $f \in L^2(\Omega)$, κ represents the permeability field that varies over multiple spacial scales. Possible applications of (1a)-(1c) include flows in porous media, diffusion and transport of passive chemicals or heat transfer in heterogeneous media. Solving (1a)-(1c) can be challenging if Ω is large and the permeability κ is heterogeneous with multiple scales and high contrast, which is a common characteristic in many industrial, scientific, engineering, and environmental applications. Direct simulation requires very fine meshes and this makes the corresponding algebraic system very large and ill conditioned (due to both

*Department of Mathematics, The Chinese University of Hong Kong, Hong Kong SAR.

[†]Department of Mathematics, Texas A&M University, College Station, TX 77843.

[‡]Department of Mathematics, Texas A&M University, College Station, TX 77843.

the small mesh size and the high contrast of the coefficient). Thus direct simulation is computationally intractable.

In order to solve (1a)-(1c) efficiently, various reduced-order methods have been proposed and applied. These methods include numerical upscaling (see, e.g.,[46, 17]), variational multiscale method (see, e.g.,[30, 31]), multiscale finite element method (see, e.g.,[18, 21, 2, 13]), mixed multiscale finite element methods (see, e.g., [11, 9]), the multiscale finite volume method (see, e.g.,[32]), mortar multiscale finite element method (see, e.g.,[45, 44, 3, 5]), multiscale hybrid-mixed finite element methods (see, e.g.,[1, 29]), generalized multiscale finite element methods (see, e.g., [19, 10, 14, 27, 12]) and weak Galerkin generalized multiscale finite element method [37]. These methods typically use some type of global couplings in the coarse grid level to link the sub-grid variations of neighboring coarse regions. We will, in this paper, consider the global coupling via the mortar framework. The mortar framework offers many advantages, such as the flexibility in the constructions of the coarse grid and sub-grid capturing tools. The framework also gives a smaller dimensional global system since the degrees of freedom are reduced to coarse region boundaries. The connectivity of the sub-grid variations is typically enforced using a Lagrange multiplier. For multiscale problems, the choice of the mortar space for the Lagrange multiplier requires a very careful construction, in order to obtain an efficient and robust method. To construct an accurate mortar space with a small dimension, we will apply the recently developed GMsFEM, which offers a systematic approach for model reduction. In particular, we first create a local snapshot space for every coarse edge. We obtain this space by first solving some local problems on a small region containing an edge, and then restricting the solutions to the edge. Next, we select the dominated modes within the snapshot space using an appropriate POD technique. These dominated modes form the basis for the mortar space. We will apply our mortar space in two related formulations. The first one is a mixed GMsFEM using the mortar formulation. This method gives a coarse-grid solver for the problem (1a)-(1c). The second one is a coarse space for some preconditioners applied to the fine scale discretization of (1a)-(1c).

In multiscale finite element method, the local basis functions are constructed independently in each coarse cell (subregion). In general, the basis functions are discontinuous across the cell interfaces. These discontinuities can be coupled by mortar spaces. The pioneering work on mixed finite element approximations on multiblock grids were introduced and studied by Arbogast et al. in ([4]). In the mortar framework, a Lagrange multiplier is introduced to impose the continuity of flux across block interfaces. This Lagrange multiplier lives in an auxiliary space (called mortar space). In a two-scale method the aim is to resolve the local heterogeneities on the fine grid introduced on each coarse block and then "glue" these approximations together via mortar spaces. The global problem is then formulated in terms of the Lagrange multiplier, which in general yields a much smaller algebraic system compared with the original systems.

If the mortar space is small, we can solve the final algebraic system relatively efficiently. However the continuity of the flux is only weakly imposed. Therefore, for both efficiency and accuracy, it is preferable to construct a mortar space that is not too large and can still impose the continuity accurately. Our goal of this work is to construct such a mortar space by a systematic enrichment technique using GMsFEM. We will first create local snapshot spaces and then perform POD to the snapshot spaces to identify important modes to form the enriched multiscale mortar space. In this way, only a few degrees of freedom per interface are used and the basis functions in the space demonstrate a good "gluing" behavior. We will also study the effects of using oversampling techniques, randomized snapshots and different sizes of local problem domain on the robustness and accuracy of our mortar space. Our work share some similarities with multiscale hybridizable discontinuous Galerkin method [23, 22], but the key part is different, which involves the use of a new methodology to construct basis. The mortar mixed finite element enjoys the advantage of global mass conservation, which is important in industrial reservoir simulations.

On the other hand, based on our proposed mortar space, we will construct an effective and robust two-level preconditioner to solve the algebraic system arising from a fine scale discretization by some iterative methods. Our approach uses the solutions of small local problems and a coarse problem in constructing the preconditioners for the fine-scale system. It is well known that for high contrast heterogeneous media, if the coarse problem is not suitably chosen, the performance of the preconditioner may deteriorate. To

deal with this problem, many researchers designed different types of robust two-level preconditioners with nonstandard coarse problems in the past several decades. For example, in [41] the authors proposed a nonstandard coarse space for the elliptic problems with discontinuous coefficients. The idea of using single multiscale basis to form the coarse space is reported in [28, 38], this method is robust if the high conductivity does not cross the coarse grid. Using spectral functions to enrich the coarse space turns out to be very efficient and robust for problems with almost any types of media (see, e.g., [24, 25, 20, 16, 35, 42, 33, 34, 36, 39]).

Following previously mentioned works, we propose a two-level preconditioner which utilizes the multiscale mortar space designed in this paper to construct the coarse preconditioner. The local preconditioner is formed by solving a local Dirichlet problem in the neighborhood of each edge. This local preconditioner will be block diagonal and is more effective for highly heterogeneous coefficient than the coarse element based local preconditioner, see [47]. However, neighborhood defined local preconditioner may lead to higher computational cost. To solve this problem, we will also consider restrictive local preconditioner [7], which is quite similar to the oversampling techniques when constructing the multiscale basis. Moreover, we will study the effects of the size of local problems and robustness of the method. We remark that the preconditioners designed in this paper is similar to the one in [6, 47], the major difference is the construction of the coarse space. In [6], polynomials and homogenized basis functions are applied for the coarse preconditioner, which shows good performance for checker board type high-contrast model, however there is no evidence that the polynomial or homogenized basis functions can deal with arbitrary type of high contrast media. Our numerical results show that the proposed coarse space gives promising ability to deal with problems in media with complicated inclusions and long channels that may cross coarse edges.

The paper is organized as follows. In section 2, we first describe the coarse and fine discretizations of the domain, then present the framework of mortar mixed finite element method, followed by the description of the domain decomposition method. In section 3, we introduce the construction of the multiscale basis. In section 4, the coarse and local preconditioners are defined, which are combined to form our two-level preconditioners. Numerical examples are given in section 5, and conclusions are made in the last section.

2 Preliminaries

In this section, we will give some basic definitions. We will also present the formulations of a fine-scale discretization for (1a)-(1c) and its domain decomposition formulation, as well as the formulation for a mixed multiscale method for (1a)-(1c).

2.1 Fine and coarse grids

The proposed multiscale mortar space requires a coarse grid and a fine grid, which will be introduced in this section. We first divide the computational domain Ω into non-overlapping polygonal coarse blocks K_i with diameter H_i so that $\bar{\Omega} = \cup_{i=1}^N \bar{K}_i$, where N is the number of coarse blocks. The decomposition of the domain can be nonconforming. We call E a coarse edge of the coarse block K_i if $E = \partial K_i \cap \partial K_j$ or $E_H = \partial K_i \cap \partial \Omega$. Let $\mathcal{E}_H(K_i)$ be the set of all coarse edges on the boundary of the coarse block K_i and $\mathcal{E}_H = \cup_{i=1}^N \mathcal{E}_H(K_i)$ be the set of all coarse edges.

For each coarse block K_i , we introduce a shape regular discretization $\mathcal{T}_h(K_i)$ with rectangular elements (denoted as $T_j, j = 1, \dots, i_n$) with mesh size h_i . Let $\mathcal{T}_h = \cup_{i=1}^N \mathcal{T}_h(K_i)$ be the union of all these triangulations, which is a fine mesh triangulation of the domain Ω . We use h to denote the mesh size of \mathcal{T}_h . In addition, we let $\mathcal{E}_h(K_i)$ be the set of all edges of the triangulation $\mathcal{T}_h(K_i)$ and $\mathcal{E}_h^0(K_i)$ be the set of all interior edges of the triangulation $\mathcal{T}_h(K_i)$ and let $\mathcal{E}_h = \cup_{i=1}^N \mathcal{E}_h(K_i)$ be the set of all edges in the triangulation \mathcal{T}_h . We denote the edges of this triangulation by generically by e . Figure 1 gives an illustration of the constructions of the two grids. The black lines represent the coarse grid, and the grey lines represent the fine grid. For each coarse edge E_i , we define a coarse neighborhood ω_i as the union of all coarse blocks having the edge E_i . Figure 1 shows a coarse neighborhood ω_i in orange color.

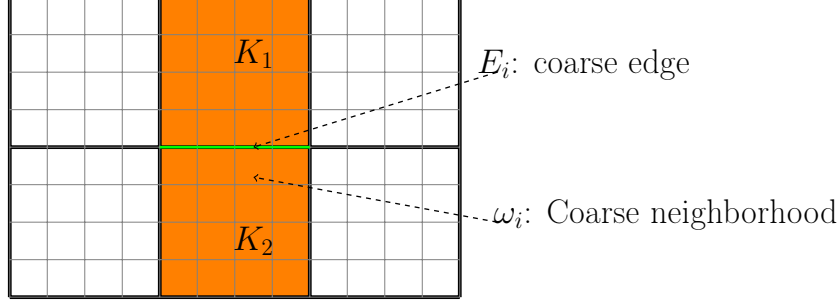


Figure 1: Illustration of the coarse and fine grids and a coarse neighborhood.

2.2 Fine scale mortar mixed finite element method

In this section, we recall the standard mortar mixed finite element method defined on the fine grid. First of all, using the two-scale grid defined in the last subsection, we define the following finite element spaces:

$$\begin{aligned}
W_h &:= \{w \in L^2(\mathcal{T}_h) : w|_T \in P^0(T), T \in \mathcal{T}_h\}, \\
\mathbf{V}_h &:= \{\mathbf{v} \in \mathbf{L}^2(\mathcal{T}_h) : \mathbf{v}|_T \in H(\text{div}; T), T \in \mathcal{T}_h\}, \\
M_h &:= \{\mu \in L^2(\mathcal{E}_h) : \mu|_e \in P^0(e), \text{ for } e \in \mathcal{E}_h \text{ and } \mu|_{\partial\Omega} = 0\}, \\
M_H &:= \{\mu \in L^2(\mathcal{E}_H) : \mu|_E \in P^0(E), \text{ for } E \in \mathcal{E}_H \text{ and } \mu|_{\partial\Omega} = 0\}, \\
M_h^0 &:= \{\mu \in L^2(\mathcal{E}_h) : \mu|_e \in P^0(e), \text{ for } e \in \mathcal{E}_h^0 \text{ and } \mu|_{\partial T} = 0\}, \\
M_H^f &:= \{\mu \in M_h, \mu \notin M_h^0\}, \\
M_{h,H} &:= M_h^0 \oplus M_H,
\end{aligned}$$

where $P^0(S)$ is the space of constant functions defined on the set S . Note that M_H is a subspace of M_H^f . Then, the fine scale mortar finite element method reads as: find $\mathbf{q}_h \in \mathbf{V}_h$, $u_h \in W_h$, and $\lambda_{h,H} \in M_{h,H}$ such that,

$$(\kappa^{-1} \mathbf{q}_h, \mathbf{v})_{\mathcal{T}_h} - (u_h, \nabla \cdot \mathbf{v})_{\mathcal{T}_h} + \langle \lambda_{h,H}, \mathbf{v} \cdot \mathbf{n} \rangle_{\partial\mathcal{T}_h} = 0 \quad \mathbf{v} \in \mathbf{V}_h \quad (2a)$$

$$\langle \nabla \cdot \mathbf{q}_h, w \rangle_{\partial\mathcal{T}_h} = (f, w)_{\mathcal{T}_h} \quad w \in W_h \quad (2b)$$

$$\langle \mathbf{q}_h \cdot \mathbf{n}, \mu \rangle_{\partial\mathcal{T}_h} = 0 \quad \mu \in M_{h,H} \quad (2c)$$

where \mathbf{n} is the outer normal unit vector. The inner product $(\eta, \xi)_{\mathcal{T}_h} = \sum_{T \in \mathcal{T}_h} (\eta, \xi)_T$, where $(\eta, \xi)_T$ denotes the L^2 inner product of η and ξ over the domain T , $\langle \eta, \xi \rangle_{\partial\mathcal{T}_h} = \sum_{T \in \mathcal{T}_h} \langle \eta, \xi \rangle_{\partial T}$, where $\langle \eta, \xi \rangle_{\partial T}$ denotes the L^2 inner product of η and ξ over the boundary ∂T of the domain T .

2.3 Domain decomposition formulation

The mortar multiscale method and the preconditioner developed in this paper are based on a domain decomposition formulation of (2a)-(2c). We will present the mortar multiscale method in this section, and derive the preconditioner in Section 4. The main feature of the mortar mixed finite element method is that it could be implemented by just solving a global system on the coarse mesh together with the solutions of some local problems. To achieve this, we split (2c) into two equations by testing separately with $\mu \in M_h^0$ and $\mu \in M_H$ so that

$$\langle \mathbf{q}_h \cdot \mathbf{n}, \mu \rangle_{\partial\mathcal{T}_h} = 0 \quad \mu \in M_h^0, \quad (3)$$

and

$$\langle \mathbf{q}_h \cdot \mathbf{n}, \mu \rangle_{\partial K_i} = 0 \quad \mu \in M_H. \quad (4)$$

We can implement the solution of Eq.(3) independently on each subdomain K_i . More specifically, for a particular subdomain K_i , let $\lambda_{h,H} = \xi_H \in M_H$. Then we can find the solution $(u_h, \mathbf{q}_h, \lambda_{h,H})|_{K_i}$ by restricting Eq.(2) to K_i :

$$(\kappa^{-1} \mathbf{q}_h, \mathbf{v})_{\mathcal{T}_h(K_i)} - (u_h, \nabla \cdot \mathbf{v})_{\mathcal{T}_h(K_i)} + \langle \lambda_{h,H}, \mathbf{v} \cdot \mathbf{n} \rangle_{\partial \mathcal{T}_h(K_i)} = 0 \quad (5a)$$

$$\langle \nabla \cdot \mathbf{q}_h, w \rangle_{\partial \mathcal{T}_h(K_i)} = (f, w)_{\mathcal{T}_h(K_i)} \quad (5b)$$

$$\langle \mathbf{q}_h \cdot \mathbf{n}, \mu \rangle_{\partial \mathcal{T}_h(K_i)} = 0 \quad (5c)$$

$$\lambda_{h,H} = \xi_H \quad (5d)$$

for all $(w, \mathbf{v}, \mu) \in W_h|_{\Omega_i} \times \mathbf{V}_h|_{K_i} \times M_h^0|_{\mathcal{E}_h^0(K_i)}$. Using the superposition principle the solution of Eq. (5c) can be further split into two parts, namely,

$$(\mathbf{q}_h, u_h, \lambda_{h,H}) = (\mathbf{q}_h(f), u_h(f), \lambda_{h,H}(f)) + (\mathbf{q}_h(\xi_H), u_h(\xi_H), \lambda_{h,H}(\xi_H)), \quad (6)$$

where $(\mathbf{q}_h(f), u_h(f), \lambda_{h,H}(f))$ satisfies

$$(\kappa^{-1} \mathbf{q}_h(f), \mathbf{v})_{\mathcal{T}_h(K_i)} - (u_h(f), \nabla \cdot \mathbf{v})_{\mathcal{T}_h(K_i)} + \langle \lambda_{h,H}(f), \mathbf{v} \cdot \mathbf{n} \rangle_{\partial \mathcal{T}_h(K_i)} = 0 \quad (7a)$$

$$\langle \nabla \cdot \mathbf{q}_h(f), w \rangle_{\partial \mathcal{T}_h(K_i)} = (f, w)_{\mathcal{T}_h(K_i)} \quad (7b)$$

$$\langle \mathbf{q}_h(f) \cdot \mathbf{n}, \mu \rangle_{\partial \mathcal{T}_h(K_i)} = 0 \quad (7c)$$

$$\lambda_{h,H}(f) = 0 \quad (7d)$$

for all $(w, \mathbf{v}, \mu) \in W_h|_{K_i} \times \mathbf{V}_h|_{K_i} \times M_h^0|_{\mathcal{E}_h^0(K_i)}$ and $(\mathbf{q}_h(\xi_H), u_h(\xi_H), \lambda_{h,H}(\xi_H))$ satisfies

$$(\kappa^{-1} \mathbf{q}_h(\xi_H), \mathbf{v})_{\mathcal{T}_h(K_i)} - (u_h(\xi_H), \nabla \cdot \mathbf{v})_{\mathcal{T}_h(K_i)} + \langle \lambda_{h,H}(\xi_H), \mathbf{v} \cdot \mathbf{n} \rangle_{\partial \mathcal{T}_h(K_i)} = 0 \quad (8a)$$

$$\langle \nabla \cdot \mathbf{q}_h(\xi_H), w \rangle_{\partial \mathcal{T}_h(K_i)} = 0 \quad (8b)$$

$$\langle \mathbf{q}_h(\xi_H) \cdot \mathbf{n}, \mu \rangle_{\partial \mathcal{T}_h(K_i)} = 0 \quad (8c)$$

$$\lambda_{h,H}(\xi_H) = \xi_H \quad (8d)$$

for all $(w, \mathbf{v}, \mu) \in W_h|_{K_i} \times \mathbf{V}_h|_{K_i} \times M_h^0|_{\mathcal{E}_h^0(K_i)}$.

Then Eq. (5) can be reduced to finding $\xi \in M_H$ such that

$$a_H(\xi_H, \mu) = g_H(\mu) \quad \text{for all } \mu \in M_H, \quad (9)$$

where the bilinear form $a_H(\xi_H, \mu) : M_H \times M_H \rightarrow R$ and the linear form $g_H(\mu) : M_H \rightarrow R$ are defined as

$$a_H(\xi_H, \mu) := \sum_{i=1}^N \langle \lambda_{h,H}(\xi_H), \mu \rangle_{\partial K_i} \quad \text{and} \quad g_H(\mu) := - \sum_{i=1}^N \langle \lambda_{h,H}(f), \mu \rangle_{\partial K_i}. \quad (10)$$

The interface bilinear form $a_H(\cdot, \cdot)$ is symmetric and positive semi-definite on M_H and this system can be solved by preconditioned conjugate gradient method. See [3, 15, 40] and reference therein for more details. We will construct a preconditioner for (9) in Section 4. On the other hand, the mortar space M_H in (9) is not accurate enough for problems with high contrast heterogeneous media. Thus, in the next section, we will introduce a multiscale mortar space for (9). In particular, we will replace the space M_H by our multiscale mortar space.

3 Multiscale mortar space

In this section, we present the construction of our multiscale mortar space. The space can be used as an approximation space for a multiscale mortar method in (9), and as a coarse solver for a class of

preconditioners, which will be presented in Section 4. Our multiscale mortar space consists of a set of multiscale basis functions, which are defined only on the coarse skeleton \mathcal{E}_H . To construct these basis functions, we will first define a set of snapshot functions for each coarse edge. The snapshots represent various modes of the solutions, and are typically large. To find the snapshots, we will solve some local problems in a small subdomain covering an edge, and then restrict the solutions to the edge. We will next define some PODs and use them to extract dominant modes within the snapshot space. These dominant modes form the multiscale basis functions. Notice that these basis functions capture some information of the permeability field within neighboring coarse blocks of an edge.

Construction of local snapshot space $V_{\text{snap}}^E(\omega_i)$.

Let $E_i \in \mathcal{E}_H^0$ be an interior edge and let ω_i be the corresponding coarse neighborhood covering E_i (see Figure 1). We will first construct a set of local snapshots $\{\psi_j^{E_i}\}_{j=1}^{N_i}$ defined on ω_i and

$$V_{\text{snap}}^{E_i}(\omega_i) = \text{span}\{\psi_j^{E_i}\}_{j=1}^{N_i}.$$

The snapshots can be given explicitly or computed via solutions of local boundary value or local spectral problems in ω_i . We will in this paper use the following approach. For each coarse edge E_i , we define

$$W_i(\partial\omega_i) = \{w_j^i \mid w_j^i = 1 \text{ on } e_j; \quad w_j^i = 0 \text{ on } \partial\omega_i - e_j, 1 \leq j \leq N_{\omega_i}\},$$

where N_{ω_i} is the number of fine edges on $\partial\omega_i$, and e_j is the j -th fine edge on $\partial\omega_i$. To construct the snapshots, we solve the following problem

$$-\nabla \cdot (\kappa \nabla u_j^i) = 0, \quad \text{in } \omega_i, \quad (11)$$

$$u_j^i = w_j^i, \quad \text{on } \partial\omega_i. \quad (12)$$

Using the solutions of the above problem, we obtain the space $\{\psi_j^E = u_j^i|_{E_i}, j = 1, \dots, N_{\omega_i}\}$. Finally, we obtain the snapshot space $V_{\text{snap}}^E(\omega_i) = \text{span}\{\psi_j^E\}$.

Construction of multiscale mortar space V_{off}^E .

To construct our multiscale mortar space, we will apply a space reduction technique to the snapshot space $V_{\text{snap}}^{E_i}(\omega_i)$ to obtain a smaller dimensional space. In particular, we will perform POD to $V_{\text{snap}}^{E_i}(\omega_i)$ and then select the first l_i dominant modes Ψ_j^i . In this way, we obtain the offline space corresponding to the coarse face E_i , which is

$$V^E(E_i) = \text{span}\{\Psi_j^i, 1 \leq j \leq l_i\}. \quad (13)$$

To simplify the notations, we use the single-index notation:

$$V_{\text{off}}^E = \text{span}\{\Psi_i^{\text{off}} : 1 \leq i \leq M_{\text{off}}\},$$

where $M_{\text{off}} = \sum_{i=1}^{N_e} J_i$. We define

$$R_{\text{off}}^E = [\psi_1^{\text{off}}, \dots, \psi_{M_{\text{off}}}^{\text{off}}],$$

which maps from the offline space to the fine space, and ψ_i^{off} is a vector containing the coefficients in the expansion of Ψ_i^{off} in the fine-grid basis functions. We use this multiscale offline basis to enrich the constant mortar space M_H , and use the resulting space to solve (9).

Oversampling and randomized snapshot.

One can use an oversampling technique to improve the accuracy of the method. The main idea of the oversampling approach is to use larger domains ω_i^+ instead of ω_i to compute snapshot, see Figure 3 for examples of oversampling domain of a coarse edge. A typical choice of $V_{\text{snap}}^E(\omega_i)$ is local flow solutions, which are constructed by solving local problems with all possible boundary conditions. This can be expensive and for this reason, one can use randomized boundary conditions (see [8]) and construct only a few more snapshots than the number of desired local basis functions.

4 Two-level domain decomposition preconditioners

Previous sections are devoted to the design a good multiscale mortar space to achieve a desired accuracy. In this section, we will apply our multiscale mortar space for an iterative method applied to solve the fine scale system. We will describe a two-level iterative method to solve the fine scale problem with the previously introduced multiscale basis as the coarse space, see [6, 47] for the case of polynomial and homogenized multiscale basis. The two-level preconditioner B^{-1} includes two part, a local fine scale preconditioner B_{loc}^{-1} to smooth out fine-scale error and a global coarse-scale preconditioner B_0^{-1} for exchanging global information.

4.1 Global coarse preconditioners

We denote the coarse basis functions as $\{\Phi_i\}_{i=1}^{N_c}$, where N_c the total number of coarse basis functions, which is usually larger than the total number of coarse edges due to the use of enriched basis. Then we can define the coarse space as

$$V_0 = \text{span}\{\Phi_i\}_{i=1}^{N_c}$$

and the coarse matrix $A_0 = R_0 A R_0^T$, where $R_0^T = [\Phi_1, \Phi_2, \dots, \Phi_{N_c}]$, and A is the matrix corresponding to bilinear form $a_H(\xi_i, \xi_j) : M_H^f \times M_H^f \rightarrow R$ defined in (10). Then, the coarse preconditioner is defined as

$$B_0^{-1} = R_0 A_0^{-1} R_0^T.$$

The selection of coarse space V_0 is quite important to the performance of the preconditioner, we will use the multiscale basis (13) constructed in the previous section to form the mortar space V_0 .

4.2 Local preconditioners

The local preconditioner is B_{loc}^{-1} defined neighborhood wise. More specifically, Let $\mathcal{R}_i : M_H \rightarrow M_H|_{E_i}$ be the restriction operator from \mathcal{E}_H to E_i and let R_i be the corresponding matrix representation. For each coarse edge E_i , we will consider a domain $\omega_i^+ \supset E_i$ (see Figure 3 for the illustration of ω_i^+) to apply the local preconditioner. Similarly, we define the restriction operator from \mathcal{E}_H to $E_i^+ = \mathcal{E}_H \cap \omega_i^+$ as $\mathcal{P}_i : M_H \rightarrow M_H|_{E_i^+}$ and corresponding matrix P_i . Note that ω_i^+ can be the same as ω_i . Then we define the local preconditioner as

$$B_{loc}^{-1} = \sum_i R_i^T A_i^{-1} P_i,$$

where $A_i = P_i A P_i^T$. The application of A_i^{-1} is equivalent to solve a homogeneous Dirichlet boundary condition problem on ω_i^+ with local residual as source.

If $\omega_i^+ = \omega_i$, then we have $R_i = P_i$, which implies that B_{loc}^{-1} is symmetric and we can use PCG as outside accelerator. In this case, the computational cost (although it is offline) of applying local preconditioners may be expensive especially in 3D case. To reduce the computational cost, we can consider the case $\omega_i^+ \neq \omega_i$, which is actually the restrictive local preconditioner [7]. This will not only reduce the computation of applying local preconditioner, but also decrease the number of iterations since it includes the distant information. In this case B_{loc}^{-1} is no longer symmetric, and we can choose algorithm such as GMRES as the outer accelerator.

Remark 1. *Restrictive local preconditioner is quite similar with the idea of oversampling, both utilize a larger domain than standard domain to perform computation and then take restriction. Both method shows better performance than standard method.*

4.3 Two-level preconditioners

We combine the local preconditioner and coarse preconditioner in two ways to form the two-level preconditioners. The first approach is the *additive* preconditioner

$$B_{add}^{-1} = B_0^{-1} + B_{loc}^{-1}. \quad (14)$$

The second is the *hybrid* preconditioner

$$B_{\text{hyb}}^{-1} = B_0^{-1} + (I - B_0)B_{\text{loc}}^{-1}(I - B_0^T). \quad (15)$$

where $P_0 = B_0A$ is the Schwarz projection operator, see [43] for details. For more details about the two-level preconditioners we adopted here, we refer [6, 47] and reference therein. We remark again that the main ingredient in the above preconditioners is the use of our mortar multiscale space constructed in Section 3.

5 Numerical examples

In this section, we present some representative examples to show the performance of our method. We consider two models with permeability κ depicted in Figure 2. We note that $\kappa = 1$ in the blue region and $\kappa = \eta (>> 1)$ in the red region. We will consider two cases: $\eta = 10^4, \eta = 10^6$ in the following examples. As it is shown, these two models contains high contrast, short and long channels, and isolated inclusions. We will first demonstrate the performance of the multiscale solver by showing the error of multiscale solution against the fine scale (reference) solution. Next we report the results of two-level additive Schwarz domain decomposition method with the coarse space formed by using our multiscale mortar space. We will consider different snapshot space computed on different domains, and also consider various preconditioners.

We divide the domain $\Omega = (0, 1)^2$ into $N \times N$ square coarse elements. In each coarse element, we generate a uniform $n \times n$ fine scale square elements. Therefore, the domain was divided into $N_f \times N_f$ fine elements, where $N_f = N \times n$. The number of degrees of freedom for the fine solver is $5 \times N_f^2 + 2 \times N_f \times (N_f - 1)$, while the number of degree of freedom for the multiscale solver is $N_b \times 2 \times N \times (N - 1)$, where N_b is the number of multiscale basis on each coarse edge.

Constant sources and homogeneous Dirichlet boundary condition are considered. We use $\begin{pmatrix} d_{11} & d_{12} \\ d_{21} & d_{22} \end{pmatrix}$ to define local computational domain of the snapshot and the local preconditioner. See Figure 3 for the illustration of d_{ij} . In total, 4 ways to generate the multiscale space are considered:

Domain 1: No oversampling: $\begin{pmatrix} n & 0 \\ 0 & n \end{pmatrix}$

Domain 2: oversampling case a: $\begin{pmatrix} n & 1 \\ 1 & n \end{pmatrix}$

Domain 3: oversampling case b: $\begin{pmatrix} [n/2] & 1 \\ 1 & [n/2] \end{pmatrix}$

Domain 4: oversampling case c: $\begin{pmatrix} 2 & 1 \\ 1 & 2 \end{pmatrix}$

5.1 Coarse grid multiscale solution

In this subsection, we study the error decay of multiscale solution by adding more multiscale basis. We will consider using 4 types of multiscale basis as well as polynomial basis for comparison. We will demonstrate the influence of snapshot, mesh size and contrast of the permeability on the multiscale solution. We define the following error to quantify the accuracy of coarse grid multiscale solution.

$$e_u := \frac{\|u_{ms} - u_f\|_{L^2, \Omega}}{\|u_f\|_{L^2, \Omega}}, \quad e_q := \frac{\|\mathbf{q}_{ms} - \mathbf{q}_f\|_{\kappa, \Omega}}{\|\mathbf{q}_f\|_{\kappa, \Omega}}$$

where $\|\mathbf{q}\|_{\kappa, \Omega}^2 = \int_{\Omega} \kappa^{-1} \mathbf{q}^2 dx$.

The 4 types of multiscale basis based on the way of generating the snapshot are:

Case 1: full snapshot on domain 1

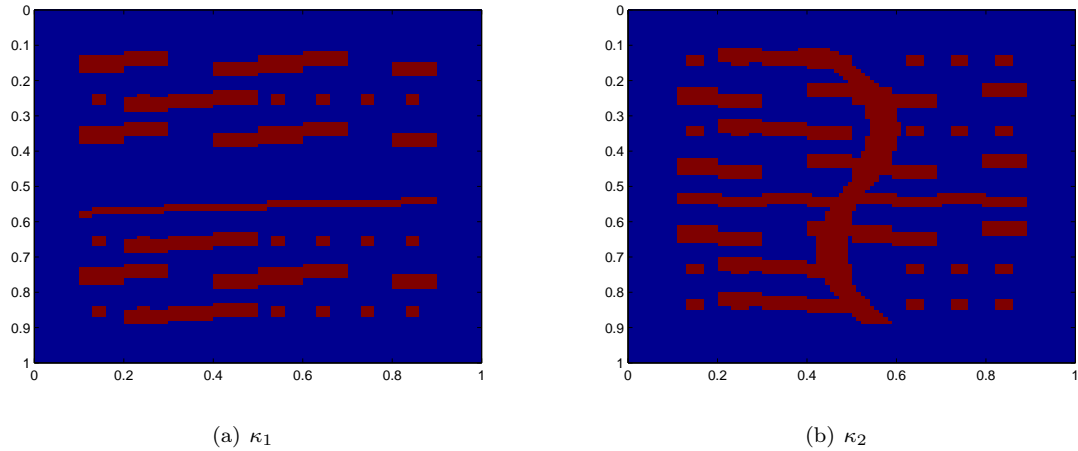


Figure 2: Permeability fields.

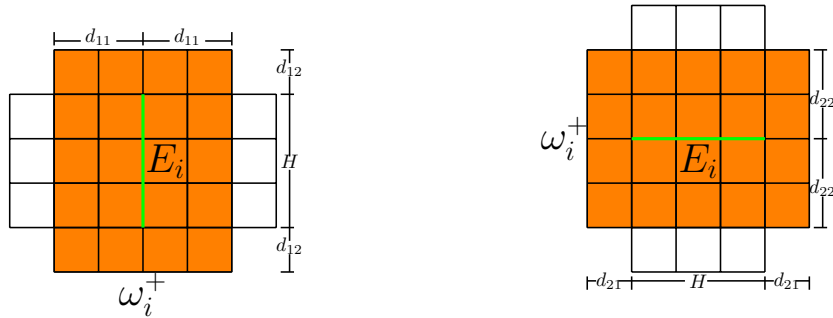


Figure 3: Illustration of an oversampled neighborhood.

Case 2: full snapshot on domain 2

Case 3: oversampling full snapshot on domain 3

Case 4: $(n + 2)$ randomized snapshot on domain 2.

Table 1 and Table 2 present the numerical results for model 1 with mesh setting $N = 5, n = 20$ and $N = 10, n = 10$ respectively. The first column is the number of multiscale basis for each coarse edge. The rest of the columns present both errors e_u, e_q for using polynomial basis, and 4 types of multiscale basis as described before. As it is shown, by adding basis, both types of errors decrease for all types of basis considered. Moreover, the error decay of all multiscale basis cases are faster than the polynomial basis case. For example, in Table 1, the relative weighted velocity error e_q decreases from 78.6% to 6.2% in case 2 when $N = 5$; however, the corresponding error decreases from 78.2% to 26.7% for polynomial basis. We remark that 6% error is tolerable in industry flow simulation. By using 5 basis on each coarse edge, the error e_u for the polynomial case is 10.3%, while this error for the multiscale basis cases are below ten percent. Note that, by using 5 basis on each coarse edge, the number of degree of freedom of multiscale solver is about 0.3% of that of the fine solver. By comparing case 1 and case 2(oversampling case), we can observe obvious improvement by applying oversampling although only 1 fine scale element is added to the snapshot domain. We remark that adding more fine scale elements to the domain of computing snapshot will further improve the solution. From the results of case 2 and case 4, we can see that the performance of randomized snapshot is also comparable with full snapshot, and it is better than case 3 and case 1. In Figure 4, for model 1, the reference solution and the corresponding multiscale solutions with different number of basis on each coarse edge are presented. The upper left is the reference solution.

The upper right is the multiscale solution with 1 basis on each coarse edge. This solution has obvious discontinuity across the coarse edges. The bottom left shows the multiscale solution with 3 basis on each coarse edge, which is closer to the reference solution. However, we can see slight difference between this solution and reference solution. The bottom right is the multiscale solution with 5 basis on each coarse edge, this solution is almost identical with the reference solution. This figure shows that the additional multiscale basis functions are important to capture all the features of the solution.

By comparing the errors in Table 1 and Table 2, we notice that smaller coarse grid size can improve the accuracy of the solution. For example, the second column in Table 1, e_u for polynomial basis drops from 63.0% to 10.3%, while the same error in Table 2 drops from 60.9% to 5.0%; the third column in Table 1, e_q for Case 1 drops from 78.6% to 8.8%, while the same error in Table 2 drops from 77.8% to 2.7%.

Table 3 and Table 4 show corresponding results for model 2. We observe similar results as model 1. Both types of errors decrease for all types of basis considered by adding more basis. The error decay of all multiscale basis cases are faster than the polynomial basis case. For example, if $N = 10$ by adding to 5 basis on each coarse edge, the error e_u for polynomial case decreases to 1.9%; while the errors for multiscale cases decrease to 0.6%, 0.04%, 1.1%, 0.08% respectively. By comparing case 1 and case 2, we can again observe obvious improvement by applying oversampling although only 1 fine scale element is added to the snapshot domain. From the results of case 2 and case 4, we can see that the performance of randomized snapshot is also comparable with full snapshot, and it is better than case 3 and case 1.

In Figure 5, for model 2, the reference solution and the corresponding multiscale solutions with different numbers of basis on each coarse edge are presented. The upper left is the reference solution. The upper right is the multiscale solution with 1 basis on each coarse edge. Apparently the solution is discontinuous across the coarse edges. The bottom left is the multiscale solution with 3 basis on each coarse edge, which shows better agreement with the reference solution. However, there are still some detailed features missing in the multiscale solution. The bottom right is the multiscale solution with 5 basis on each coarse edge, which has good agreement with the reference solution. This figure shows that the additional multiscale basis functions are important to capture all the features of the solution. These results for model 2 demonstrate that our multiscale solver can handle permeability field with long channel effects.

We also test the robustness of our method by varying the order of high contrast. The results are presented in Figure 6 and Figure 7. In Figure 6, the errors e_u (left), e_q (right) for model 1 with high contrast order $\eta = 10^4, 10^6$ with coarse $N = 5, N = 10$ are plotted. The black dashed line is for the case $10^4, N = 5$, the blue dashed line is for the case $10^6, N = 5$. The two lines are identical. The green dashed line is for the case $10^4, N = 10$, the red dashed line is for the case $10^6, N = 10$. The two lines are also identical.

Figure 7 displays the corresponding results for model 2. Though the lines do not overlap, the difference is very small. We note that the snapshot we used for both cases comes from case 2. From these examples, we see that our method produces robust results independent of the order of high contrast. Robustness will further be confirmed by our preconditioner results in following parts.

Nb	Polynomial		Case 1		Case 2		Case 3		Case 4	
	e_u	e_q	e_u	e_q	e_u	e_q	e_u	e_q	e_u	e_q
1	0.630	0.786	0.630	0.786	0.630	0.786	0.630	0.786	0.630	0.786
2	0.432	0.647	0.438	0.649	0.357	0.581	0.351	0.581	0.427	0.640
3	0.288	0.519	0.157	0.374	0.139	0.354	0.143	0.357	0.129	0.341
4	0.120	0.291	0.060	0.232	0.014	0.104	0.050	0.207	0.038	0.171
5	0.103	0.267	0.012	0.088	0.006	0.062	0.028	0.157	0.008	0.073

Table 1: Relative error between multiscale solution and fine scale solution with different types of basis for model 1, $N = 5, \eta = 10^4$. "Nb" represent the number of basis per coarse edge.

Nb	Polynomial		Case 1		Case 2		Case 3		Case 4	
	e_u	e_q	e_u	e_q	e_u	e_q	e_u	e_q	e_u	e_q
1	0.609	0.778	0.609	0.778	0.609	0.778	0.609	0.778	0.609	0.778
2	0.133	0.322	0.140	0.329	0.130	0.316	0.133	0.320	0.106	0.287
3	0.103	0.278	0.026	0.128	0.019	0.114	0.039	0.167	0.026	0.135
4	0.069	0.232	0.012	0.092	0.010	0.083	0.029	0.142	0.004	0.050
5	0.050	0.197	0.001	0.027	3.9e-04	0.013	0.002	0.035	6.7e-04	0.020

Table 2: Relative error between multiscale solution and fine scale solution with different types of basis for model 1, $N = 10$, $\eta = 10^4$. "Nb" represent the number of basis per coarse edge.

Nb	Polynomial		Case 1		Case 2		Case 3		Case 4	
	e_u	e_q	e_u	e_q	e_u	e_q	e_u	e_q	e_u	e_q
1	0.668	0.806	0.668	0.806	0.668	0.806	0.668	0.806	0.668	0.806
2	0.508	0.699	0.549	0.728	0.410	0.627	0.447	0.655	0.466	0.651
3	0.332	0.560	0.265	0.494	0.151	0.370	0.151	0.370	0.142	0.358
4	0.118	0.316	0.136	0.348	0.038	0.178	0.039	0.181	0.041	0.187
5	0.077	0.244	0.061	0.211	0.012	0.089	0.009	0.075	0.026	0.153

Table 3: Relative error between multiscale solution and fine scale solution with different types of basis for model 2, $N = 5$, $\eta = 10^4$. "Nb" represent the number of basis per coarse edge.

Nb	Polynomial		Case 1		Case 2		Case 3		Case 4	
	e_u	e_q	e_u	e_q	e_u	e_q	e_u	e_q	e_u	e_q
1	0.593	0.769	0.593	0.769	0.593	0.769	0.593	0.769	0.593	0.769
2	0.055	0.205	0.118	0.304	0.090	0.266	0.090	0.267	0.074	0.245
3	0.044	0.175	0.031	0.146	0.011	0.082	0.017	0.109	0.014	0.098
4	0.029	0.142	0.015	0.101	0.002	0.035	0.007	0.065	0.004	0.049
5	0.019	0.115	0.006	0.055	4.4e-04	0.011	0.001	0.023	7.6e-04	0.017

Table 4: Relative error between multiscale solution and fine scale solution with different types of basis for model 2, $N = 10$, $\eta = 10^4$. "Nb" represent the number of basis per coarse edge.

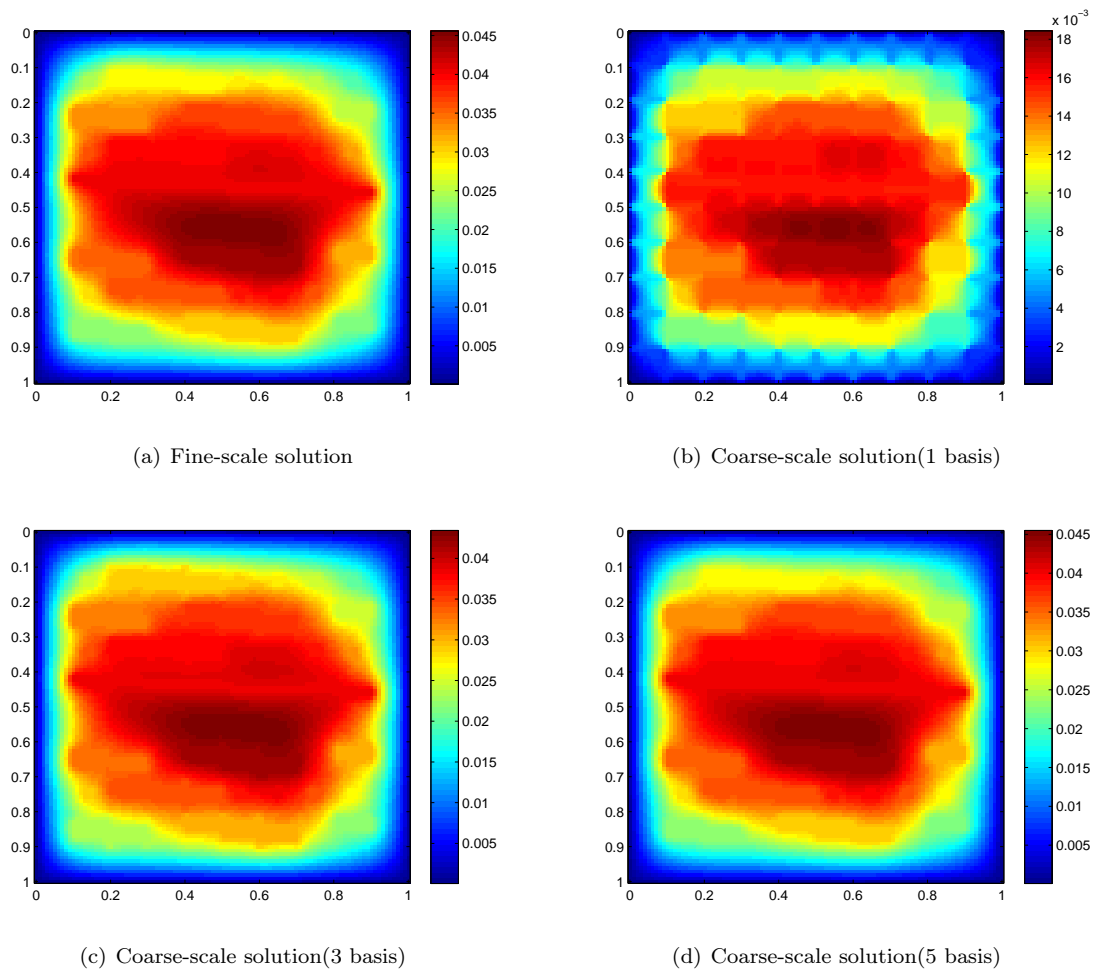
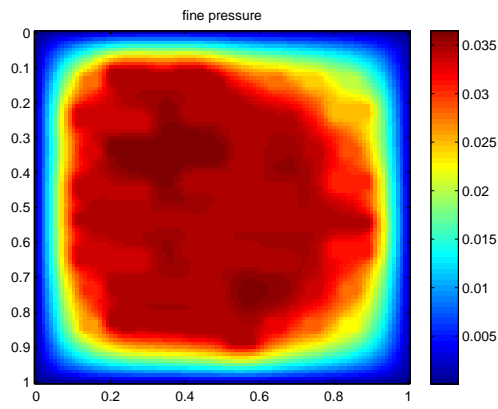
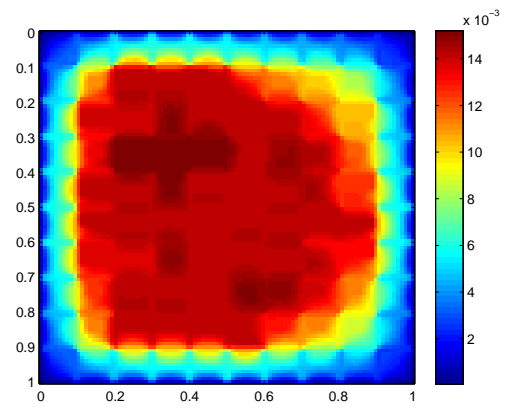


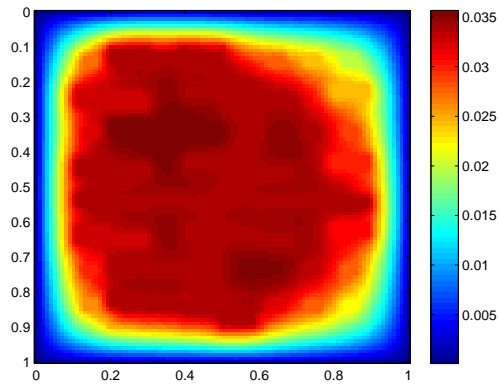
Figure 4: Comparison of the coarse-scale solutions with the reference (fine-scale) solution, $N = 10$, $\eta = 10^4$, model 1.



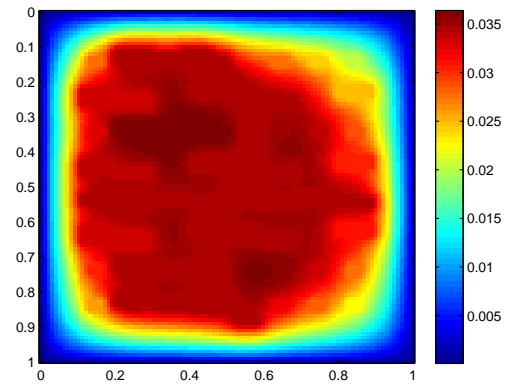
(a) Fine-scale solution



(b) Coarse-scale solution(1 basis)



(c) Coarse-scale solution(3 basis)



(d) Coarse-scale solution(5 basis)

Figure 5: Comparison of the coarse-scale solutions with the reference (fine-scale) solution, $N = 10$, $\eta = 10^4$, model 2.

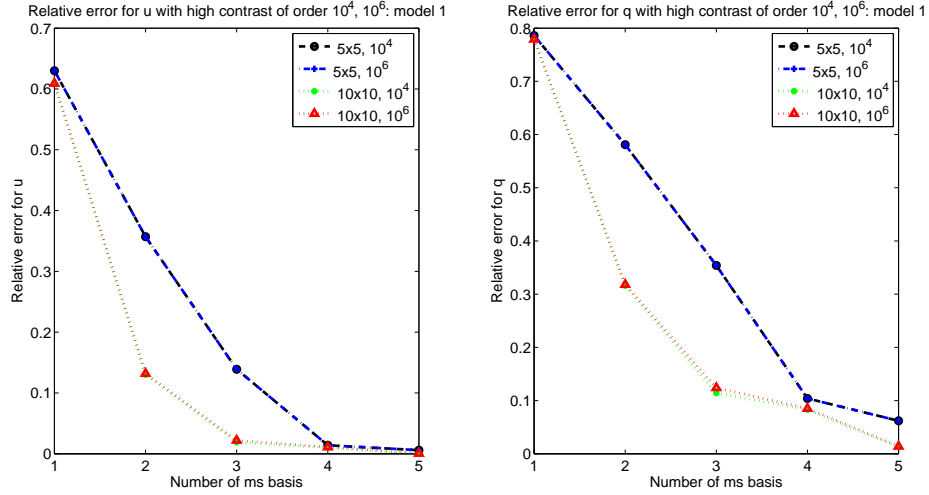


Figure 6: Relative error for u (left), q (right) with contrast order $\eta = 10^4$ and $\eta = 10^6$ for model 1, basis generation case 2.

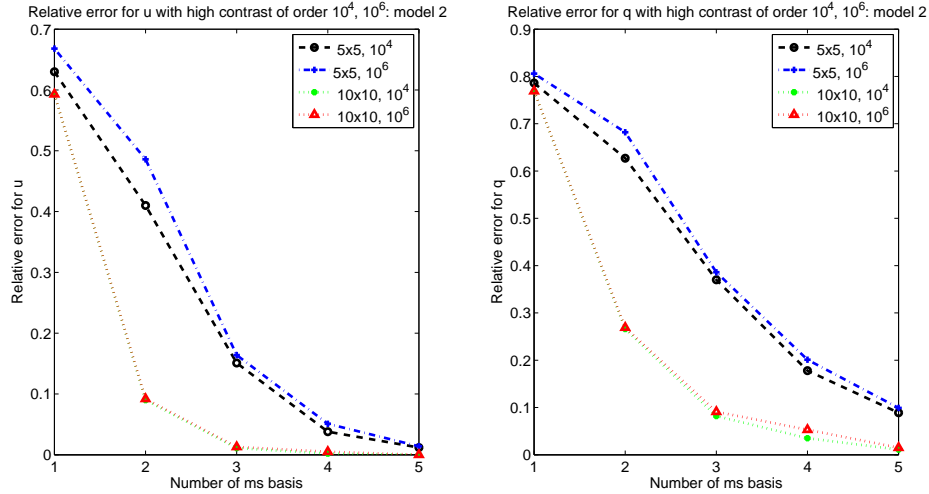


Figure 7: Relative error for u (left), q (right) with contrast order $\eta = 10^4$ and $\eta = 10^6$ for model 2, basis generation case 2.

5.2 Preconditioner

In this subsection, we present the numerical results of using multiscale basis to form the coarse space for the two level additive Schwarz domain decomposition preconditioner. We use PCG as outer accelerator if the two-level preconditioner is symmetric, otherwise GMRES with restarted number of 2 (GMRES(2)) is applied. We adopt the techniques in [26] to implement the local preconditioner M_{loc}^{-1} . Then the dominant computation can be done offline and it can be parallelized with coloring techniques, the dimension of

each local preconditioner is equal to the number of fine scale edges in the adjacent coarse elements, which is quite small and thus can be precomputed and saved. Direct solver is used to implement M_0^{-1} . We consider both additive and hybrid preconditioners. We are particularly interested in the robustness of the method, and in each simulation we consider three types of contrast to test the robustness. The initial guess is zero, and the stopping criterion that the residual is reduced by a factor of 10^7 in L^2 norm.

The first test involves comparing the PCG iteration number of using multiscale basis and polynomial basis to form coarse space of the coarse preconditioner, which is shown in Table 5. The first column gives the order of high contrast. The second column is the number of PCG iterations of using polynomial to form the coarse space. The rest of the columns give the number of PCG iterations of using multiscale basis from Case 3 and Case 4 to form the coarse space. We can see clearly that for each case, the iteration number of multiscale basis is generally much smaller than that of polynomial basis. If polynomial basis is used, the preconditioner is not robust with respect to the contrast of the media. For example, for the hybrid method in the second column, PCG iteration number is 13 for contrast 10^2 , and increases to 39 for contrast 10^6 . While for the multiscale basis, iteration number is almost independent of contrast. Hybrid preconditioner performs better than additive preconditioner in terms of iteration number, however, hybrid preconditioner requires to apply the coarse preconditioner twice in each iteration.

Next, we focus our study on the influence of the domain size on local preconditioner. In Table 6, the GMRES(2) iteration numbers of using multiscale basis from case 3 with four types of computational domain are presented. Two multiscale basis on each coarse edge is used to form the coarse space. The first column gives the order of high contrast. The rest of the columns give the number of GMRES(2) outer iterations for the four types of computational domain. As it is shown, a restrictive local preconditioner (cases of Domain 2, 3, 4) can reduce the iteration number approximately by half by comparing the results of Domain 1 and the rest of the 3 domain cases. For example, the number of iteration for the additive case from Domain 1 for contrast of order $10^2, 10^4, 10^6$ is 20, 18, 18 respectively, while from Domain 2 the number of iteration for the additive case is 10, 11, 11. Moreover, iteration number is almost independent of contrast for all types of domains. In Table 7, the GMRES(2) iteration numbers of using multiscale basis from case 4 with four types of computational domain are presented. We observed similar results as in Table 6. Since multiscale basis from case 4 uses randomized technique for snapshot, it is acceptable that the number of iterations are slightly larger than the number of iterations of corresponding cases in Table 6.

Contrast	Polynomial		Case 3		Case 4	
	additive	hybrid	additive	hybrid	additive	hybrid
10^2	23	13	25	16	26	16
10^4	> 40	28	27	16	29	17
10^6	> 40	39	27	16	28	16

Table 5: PCG iteration number with different types of coarse space, 2 basis is used for coarse space, $N = 5$.

Contrast	Domain 1		Domain 2		Doamin 3		Domain 4	
	additive	hybrid	additive	hybrid	additive	hybrid	additive	hybrid
10^2	20	10	10	5	10	5	11	6
10^4	18	10	11	5	12	5	13	7
10^6	18	10	11	5	12	5	11	6

Table 6: GMRES(2) iteration number with different types of preconditioners and different local preconditioner, 2 basis is used for coarse space with multiscale basis case 3, $N = 5$.

Contrast	Domain 1		Domain 2		Doamin 3		Domain 4	
	additive	hybrid	additive	hybrid	additive	hybrid	additive	hybrid
10^2	17	10	15	7	12	8	16	9
10^4	20	8	18	5	18	10	18	7
10^6	18	10	14	6	12	7	16	9

Table 7: GMRES(2) iteration number with different types of preconditioners and different local preconditioner, 2 basis is used for coarse space with multiscale basis case 4, $N = 5$.

6 Conclusion

We have developed an enriched multiscale mortar mixed finite element method for elliptic problems. The method is based on a mixed formulation of the problem, the concepts of domain decomposition, and mortar techniques. The multiscale basis functions are constructed from local problems. This method fully resolve the problem within the subdomains and glues them together with a coarse mortar finite element space. Further, we design both two-level *additive*, *hybrid* preconditioners which can be used within a Krylov accelerator such as PCG or GMRES. These two-level preconditioners consist of a local smoothing preconditioner based on block Jacobi(BJ), blocked by subdomain interfaces, and a coarse preconditioner based on subdomain interfaces using the enriched multiscale mortar method. Finally we present some numerical examples to demonstrate the performance of the method.

References

- [1] Rodolfo Araya, Christopher Harder, Diego Paredes, and Frédéric Valentin. Multiscale hybrid-mixed method. *SIAM Journal on Numerical Analysis*, 51(6):3505–3531, 2013.
- [2] T. Arbogast. Analysis of a two-scale, locally conservative subgrid upscaling for elliptic problems. *SIAM J. Numer. Anal.*, 42(2):576–598 (electronic), 2004.
- [3] T. Arbogast, G. Pencheva, M.F. Wheeler, and I. Yotov. A multiscale mortar mixed finite element method. *Multiscale Model. Simul.*, 6(1):319–346, 2007.
- [4] Todd Arbogast, Lawrence C Cowsar, Mary F Wheeler, and Ivan Yotov. Mixed finite element methods on nonmatching multiblock grids. *SIAM Journal on Numerical Analysis*, 37(4):1295–1315, 2000.
- [5] Todd Arbogast and Hailong Xiao. A multiscale mortar mixed space based on homogenization for heterogeneous elliptic problems. *SIAM Journal on Numerical Analysis*, 51(1):377–399, 2013.
- [6] Todd Arbogast and Hailong Xiao. Two-level mortar domain decomposition preconditioners for heterogeneous elliptic problems. *Computer Methods in Applied Mechanics and Engineering*, 292:221–242, 2015.
- [7] Xiao-Chuan Cai and Marcus Sarkis. A restricted additive Schwarz preconditioner for general sparse linear systems. *Siam journal on scientific computing*, 21(2):792–797, 1999.
- [8] V.M. Calo, Y. Efendiev, J. Galvis, and G Li. G. Randomized oversampling for generalized multiscale finite element methods. *Multiscale Model. Simul.*, 14.
- [9] Zhiming Chen and Thomas Hou. A mixed multiscale finite element method for elliptic problems with oscillating coefficients. *Mathematics of Computation*, 72(242):541–576, 2003.
- [10] Eric Chung, Yalchin Efendiev, and Thomas Y Hou. Adaptive multiscale model reduction with generalized multiscale finite element methods. *Journal of Computational Physics*, 320:69–95, 2016.

- [11] Eric T Chung, Yalchin Efendiev, and Chak Shing Lee. Mixed generalized multiscale finite element methods and applications. *Multiscale Modeling & Simulation*, 13(1):338–366, 2015.
- [12] Eric T Chung, Yalchin Efendiev, Guanglian Li, and Maria Vasilyeva. Generalized multiscale finite element methods for problems in perforated heterogeneous domains. *Applicable Analysis*, pages 1–26, 2015.
- [13] Eric T Chung and Wing Tat Leung. A sub-grid structure enhanced discontinuous Galerkin method for multiscale diffusion and convection-diffusion problems. *Communications in Computational Physics*, 14(02):370–392, 2013.
- [14] Eric T Chung, Wing Tat Leung, and Maria Vasilyeva. Mixed GMsFEM for second order elliptic problem in perforated domains. *Journal of Computational and Applied Mathematics*, 304:84–99, 2016.
- [15] Bernardo Cockburn, Jayadeep Gopalakrishnan, and Raytcho Lazarov. Unified hybridization of discontinuous Galerkin, mixed, and continuous Galerkin methods for second order elliptic problems. *SIAM Journal on Numerical Analysis*, 47(2):1319–1365, 2009.
- [16] Victorita Dolean, Frédéric Nataf, Robert Scheichl, and Nicole Spillane. Analysis of a two-level Schwarz method with coarse spaces based on local Dirichlet-to-Neumann maps. *Computational Methods in Applied Mathematics Comput. Methods Appl. Math.*, 12(4):391–414, 2012.
- [17] L.J. Durlofsky. Numerical calculation of equivalent grid block permeability tensors for heterogeneous porous media. *Water Resour. Res.*, 27:699–708, 1991.
- [18] Y. Efendiev, J. Galvis, and X.H. Wu. Multiscale finite element methods for high-contrast problems using local spectral basis functions. *Journal of Computational Physics*, 230:937–955, 2011.
- [19] Yalchin Efendiev, Juan Galvis, and Thomas Y Hou. Generalized multiscale finite element methods (GMsFEM). *Journal of Computational Physics*, 251:116–135, 2013.
- [20] Yalchin Efendiev, Juan Galvis, Raytcho Lazarov, and Joerg Willems. Robust domain decomposition preconditioners for abstract symmetric positive definite bilinear forms. *ESAIM: Mathematical Modelling and Numerical Analysis*, 46(5):1175–1199, 2012.
- [21] Yalchin Efendiev and Thomas Y Hou. *Multiscale finite element methods: theory and applications*, volume 4. Springer Science & Business Media, 2009.
- [22] Yalchin Efendiev, Raytcho Lazarov, Minam Moon, and Ke Shi. A spectral multiscale hybridizable discontinuous Galerkin method for second order elliptic problems. *Computer Methods in Applied Mechanics and Engineering*, 292:243–256, 2015.
- [23] Yalchin Efendiev, Raytcho Lazarov, and Ke Shi. A multiscale HDG method for second order elliptic equations. Part I. Polynomial and homogenization-based multiscale spaces. *SIAM Journal on Numerical Analysis*, 53(1):342–369, 2015.
- [24] Juan Galvis and Yalchin Efendiev. Domain decomposition preconditioners for multiscale flows in high-contrast media. *SIAM J. Multiscale Model. Simul.*, 8(4):1461–1483, 2010.
- [25] Juan Galvis and Yalchin Efendiev. Domain decomposition preconditioners for multiscale flows in high contrast media: reduced dimension coarse spaces. *SIAM J. Multiscale Model. Simul.*, 8(5):1621–1644, 2010.
- [26] Benjamin Ganis and Ivan Yotov. Implementation of a mortar mixed finite element method using a multiscale flux basis. *Computer Methods in Applied Mechanics and Engineering*, 198(49):3989–3998, 2009.

- [27] Longfei Gao, Xiaosi Tan, and Eric T Chung. Application of the generalized multiscale finite element method in parameter-dependent PDE simulations with a variable-separation technique. *Journal of Computational and Applied Mathematics*, 300:183–191, 2016.
- [28] IG Graham, PO Lechner, and Robert Scheichl. Domain decomposition for multiscale PDEs. *Numerische Mathematik*, 106(4):589–626, 2007.
- [29] Christopher Harder, Diego Paredes, and Frédéric Valentin. A family of multiscale hybrid-mixed finite element methods for the Darcy equation with rough coefficients. *Journal of Computational Physics*, 245:107–130, 2013.
- [30] T. Hughes, G. Feijoo, L. Mazzei, and J. Quincy. The variational multiscale method - a paradigm for computational mechanics. *Comput. Methods Appl. Mech. Engrg.*, 166:3–24, 1998.
- [31] O. Iliev, R. Lazarov, and J. Willems. Variational multiscale finite element method for flows in highly porous media. *Multiscale Modeling & Simulation*, 9.4:1350–1372, 2011.
- [32] P. Jenny, S.H. Lee, and H. Tchelepi. Multi-scale finite volume method for elliptic problems in subsurface flow simulation. *J. Comput. Phys.*, 187:47–67, 2003.
- [33] Hyea Hyun Kim, Eric Chung, and Junxian Wang. BDDC and FETI-DP algorithms with adaptive coarse spaces for three-dimensional elliptic problems with oscillatory and high contrast coefficients. *arXiv preprint arXiv:1606.07560*, 2016.
- [34] Hyea Hyun Kim, Eric Chung, and Chenxiao Xu. A BDDC algorithm with adaptive primal constraints for staggered discontinuous Galerkin approximation of elliptic problems with highly oscillatory coefficients. *To appear in J. Comp. Appl. Math.*
- [35] Hyea Hyun Kim and Eric T Chung. A BDDC algorithm with enriched coarse spaces for two-dimensional elliptic problems with oscillatory and high contrast coefficients. *SIAM J. Multiscale Model. Simul.*, 13(2):571–593, 2015.
- [36] Axel Klawonn, Patrick Radtke, and Oliver Rheinbach. FETI-DP methods with an adaptive coarse space. *SIAM Journal on Numerical Analysis*, 53(1):297–320, 2015.
- [37] Lin Mu, Junping Wang, and Xiu Ye. A weak Galerkin generalized multiscale finite element method. *Journal of Computational and Applied Mathematics*, 305:68–81, 2016.
- [38] Duk-Soon Oh. An overlapping Schwarz algorithm for Raviart-Thomas vector fields with discontinuous coefficients. *SIAM Journal on Numerical Analysis*, 51(1):297–321, 2013.
- [39] Duk-Soon Oh, Olof B Widlund, Stefano Zampini, and Clark R Dohrmann. BDDC algorithms with deluxe scaling and adaptive selection of primal constraints for Raviart-Thomas vector fields. Technical report, tech. rep., Courant Institute, New York University, 2015. TR2015-978, 2016.
- [40] Gergina Pencheva and Ivan Yotov. Balancing domain decomposition for mortar mixed finite element methods. *Numerical linear algebra with applications*, 10(1-2):159–180, 2003.
- [41] Marcus Sarkis. Nonstandard coarse spaces and Schwarz methods for elliptic problems with discontinuous coefficients using non-conforming elements. *Numerische Mathematik*, 77(3):383–406, 1997.
- [42] Nicole Spillane, Victorita Dolean, Patrice Hauret, Frédéric Nataf, Clemens Pechstein, and Robert Scheichl. Abstract robust coarse spaces for systems of PDEs via generalized eigenproblems in the overlaps. *Numerische Mathematik*, 126(4):741–770, 2014.
- [43] Andrea Toselli and Olof Widlund. *Domain decomposition methods: algorithms and theory*, volume 34. Springer, 2005.

- [44] M.F. Wheeler, T. Wildey, and I. Yotov. A multiscale preconditioner for stochastic mortar mixed finite elements. *Comput. Methods Appl. Mech. Engrg.*, 200(9-12):1251–1262, 2011.
- [45] M.F. Wheeler, G. Xue, and I. Yotov. A multiscale mortar multipoint flux mixed finite element method. *ESAIM Math. Model. Numer. Anal.*, 46(4):759–796, 2012.
- [46] X.H. Wu, Y. Efendiev, and T.Y. Hou. Analysis of upscaling absolute permeability. *Discrete and Continuous Dynamical Systems, Series B.*, 2:158–204, 2002.
- [47] Hailong Xiao. *Multiscale mortar mixed finite element methods for flow problems in highly heterogeneous porous media*. PhD thesis, 2013.